Front. Earth Sci. 2021, 15(4): 754–769
https://doi.org/10.1007/s11707-020-0868-3

RESEARCH ARTICLE

Characteristics and formation mechanism of siltstone-mudstone rhythmic sedimentary sections in the Lower Silurian Longmaxi Formation in the Changning area, South Sichuan Basin, southwest China

Gaoxiang WANG[1,2], Lei CHEN (✉)[1], Yang YANG[3], Cui JING[3], Man CHEN[3], Xiucheng TAN[1], Xin CHEN[1], Di CAO[1], Zibo WEI[1], Minglong LI[1], Dong HUANG[4,5,6]

1 School of Geoscience and Technology, Southwest Petroleum University, Chengdu 610500, China
2 PetroChina Southwest Oil & Gasfield Company, Chengdu 610051, China
3 Sichuan Changning Natural Gas Development Co. Ltd, Chengdu 610051, China
4 Shale Gas Evaluation and Exploitation Key Laboratory of Sichuan Province, Chengdu 610091, China
5 Technology Innovation Center of Shale Gas Exploration and Development in Complex Structural Areas (Ministry of Natural Resources), Chengdu 610091, China
6 Sichuan Keyuan Testing Center of Engineering Technology, Chengdu 610091, China

Abstract The Lower Member of the Longmaxi Formation is generally dominated by siliceous shale, but recently we found some siltstone-mudstone rhythm sections developed in the Lower Member of the Longmaxi Formation. The study of formation mechanism of siltstone-mudstone rhythmic sedimentary sections may provide new insights into the shale sedimentary environment. Therefore, we studied the characteristics and formation mechanism of siltstone-mudstone rhythmic sedimentary sections in the Lower Member of the Longmaxi Formation in the Changning area based on core observation, thin section identification, major elements and trace elements analysis. The results show the following: 1) Two siltstone-mudstone rhythmic sedimentary sections are characterized by frequent interbed between black or gray-black shale and light gray siltstone, abundant argillaceous laminas and silty laminas, with obvious lithological boundaries having developed. Horizontal laminas and rhythmic laminas are well-developed in the shale layer, while the wavy laminas are well-developed in the siltstone layer. 2) The major compositional elements are SiO_2, Al_2O_3 and CaO, followed by Fe_2O_3, MgO, K_2O and Na_2O. 3) Compared with the world average shale, these siltstone-mudstone rhythmic sedimentary sections are rich in Mo, U and Ba, but less in V, Co, Ni, Cu. Compared with the shale layer, the siltstone layer has lower contents of V, Co and Ni. 4). The geochemical redox indices, Mo-U and CIA values suggest the formation of the siltstone-mudstone rhythmic sedimentary sections are related to influences from bottom currents in an oxic condition with a warm and humid paleoclimate.

Keywords shale, Longmaxi Formation, bottom current deposit, Sichuan Basin

1 Introduction

The black and organic-rich marine shale of the Upper Ordovician Wufeng-Lower Silurian Longmaxi Formation in Sichuan Basin, characterized by great thickness, wide distribution, high total organic carbon (TOC) content, high total gas content, brittle minerals, richness and moderate burial depth, and regarded as the most favorable strata for the exploration and development of marine shale gas in China (Zou et al., 2010; Chen et al., 2015a; Zou et al., 2015; Wang et al., 2016; Zou et al., 2016; Shan et al., 2017; Ma and Xie, 2018).Since shale gas was first obtained on an industrial scale from the Wufeng-Longmaxi Formation in the south Sichuan Basin in 2010, other shale gas fields such as Weiyuan, Changning, Fuling, Zhaotong, Luzhou

Received August 22, 2020; accepted December 23, 2020

E-mail: cl211@126.com

and Wuxi have been discovered across China (Dai et al., 2014; Guo and Zhang, 2014; Jiang et al., 2017; Chen et al., 2020; Qiu and Zou, 2020; Shu et al., 2020). It is generally believed that the Wufeng-Longmaxi shale is deposited in a low-energy, under-compensated and anoxic deep water restricted environment in Sichuan Basin (Algeo et al., 2016; Zhao et al., 2017; Yan, et al., 2019). As related studies and explorations achieved progress, it became known that anoxic deep water environment is not the only sedimentary environment where marine shale may be found. The organic-rich shale could also be deposited in shallow water areas (Macquaker, et al., 2010; Smith et al., 2019; He et al., 2020). Some scholars have found that centimeter-subcentimeter-scale bioturbation occurred in the organic-rich shale, suggesting that long-term anoxic water column is not a prerequisite for the enrichment of organic matter (Macquaker et al., 2010; Aplin and Macquaker, 2011). Other researchers have confirmed that biological deposition (Wang et al., 2014a), storm deposition (Drummond and Sheets, 2001) and bottom current deposition (Lu et al., 2017) could take place during the deposition and formation process of organic-rich shales. There are preliminary studies mainly focused on the formation mechanism of the lower part organic-rich shale in the Wufeng-Longmaxi Formation, and a general viewpoint is that biological deposition and suspended deposition at the bottom of the Longmaxi Formation is related to the the formation of high-quality organic-rich siliceous shale (Han et al., 2019; Yan et al., 2018), while storm deposition is associated with the grading sedimentary structure of the shell limestone in Guanyinqiao Member (Zhao et al., 2016). Calcareous laminas shale was developed in the middle and upper part of Longmaxi Formation with wavy laminas and cross-laminas, indicating that the sedimentary process of the shale involved bottom currents. Shale with wavy laminas at the upper part of the Longmaxi Formation is characterized by siltstone interbedded with shale, suggesting that periodic high-energy events occurred during the shale depositional process (Wang et al., 2014b). Some proposals put forth attempting to explain this phenomenon, include gravity flow, storm deposition or bottom flow (Li et al., 2016; Liang et al., 2016; Ma et al., 2016; Zhao et al., 2017). However, there is still no report related to the siltstone sections in the organic-rich shale sections at the bottom of the Longmaxi Formation.

Recently, from three drilling wells (N1, N2 and N3) in the South Sichuan Basin we found some siltstone-mudstone rhythmic sedimentary sections that had developed in the Low Member of the Longmaxi Formation, which are characterized by frequent interbed between black or gray-black shale and light gray siltstone. For this paper, two siltstone-mudstone rhythmic sedimentary sections (Section-A: 2453.93−2454.25 m; Section-B: 2460.96−2461.54 m) from the Lower Member of the Longmaxi Formation in the N1 well in South Sichuan Basin were studied. The characteristics, palaeoenvironment and the formation mechanism of these two siltstone-mudstone rhythmic sedimentary sections were analyzed through the drilling core, thin section, and analysis of major element and trace elements.

2 Geological setting

Due to the convergence between the Cathaysia Terrane and the Yangtze Plate during the Middle Ordovician, the Yangtze Plate ushered in the foreland basin tectonic evolution stage, while the Sichuan Basin became a part of backbulge of the Yangtze Plate foreland basin (Liu et al., 2011). The Chuanzhong uplift, Qianzhong uplift and Xuefengshan uplift were formed because of the intensification of compression during the Early Silurian. Such developments subsequently led to a restricted deep-water environment formed in the Sichuan Basin and its adjacent areas surrounded by these uplifts, in which the black shale of the Wufeng-Longmaxi Formation was deposited (Chen et al., 2004; Su et al., 2009; Yan et al., 2009; Wang et al., 2015).

At the transition phase between the Ordovician and Silurian, the areas from the Upper Ordovician Wufeng Formation to the Lower Silurian Longmaxi Formation are characterized by organic-rich shale developed in the Yangtze Platform. The Wufeng Formation is divided into two parts. The lower part is composed of black organic-rich siliceous shale, with a thickness ranging from several meters to more than ten meters. And an abundance of graptolite, and radiolarian can be found. The upper part of the Wufeng Formation is the Guanyinqiao Member, which is dominated by argillaceous limestone, with a thickness of no more than one meter (Chen et al., 2004; Guo et al., 2004). The Longmaxi Formation can be divided into its Upper Member and Lower Member. The Lower Member primarily consists of black carbonaceous shale and black calcareous shale, with copious graptolite, high TOC content, plentiful pyrite and bentonite laminas (Chen et al., 2019; Su et al., 2009). The Upper Member is predominantly made up of dark-gray shale, argillaceous siltstone and gray siltstone, with bountiful laminas but lower graptolite content (Guo et al., 2004).

The drilling wells N1, N2 and N3 are located in the Changning Tectonic Belt of the Sichuan Basin (Fig. 1(a)). The cores of the Longmaxi Formation were obtained from this trio of drilling wells. Cores from the N1 well show that the Lower Member of the Longmaxi Formation is dominated by black organic-rich shale with dark-gray silty shale interbedded, while the Upper Member of the Longmaxi Formation consists of dark-gray silty shale and gray siltstone (Fig. 1(b)).

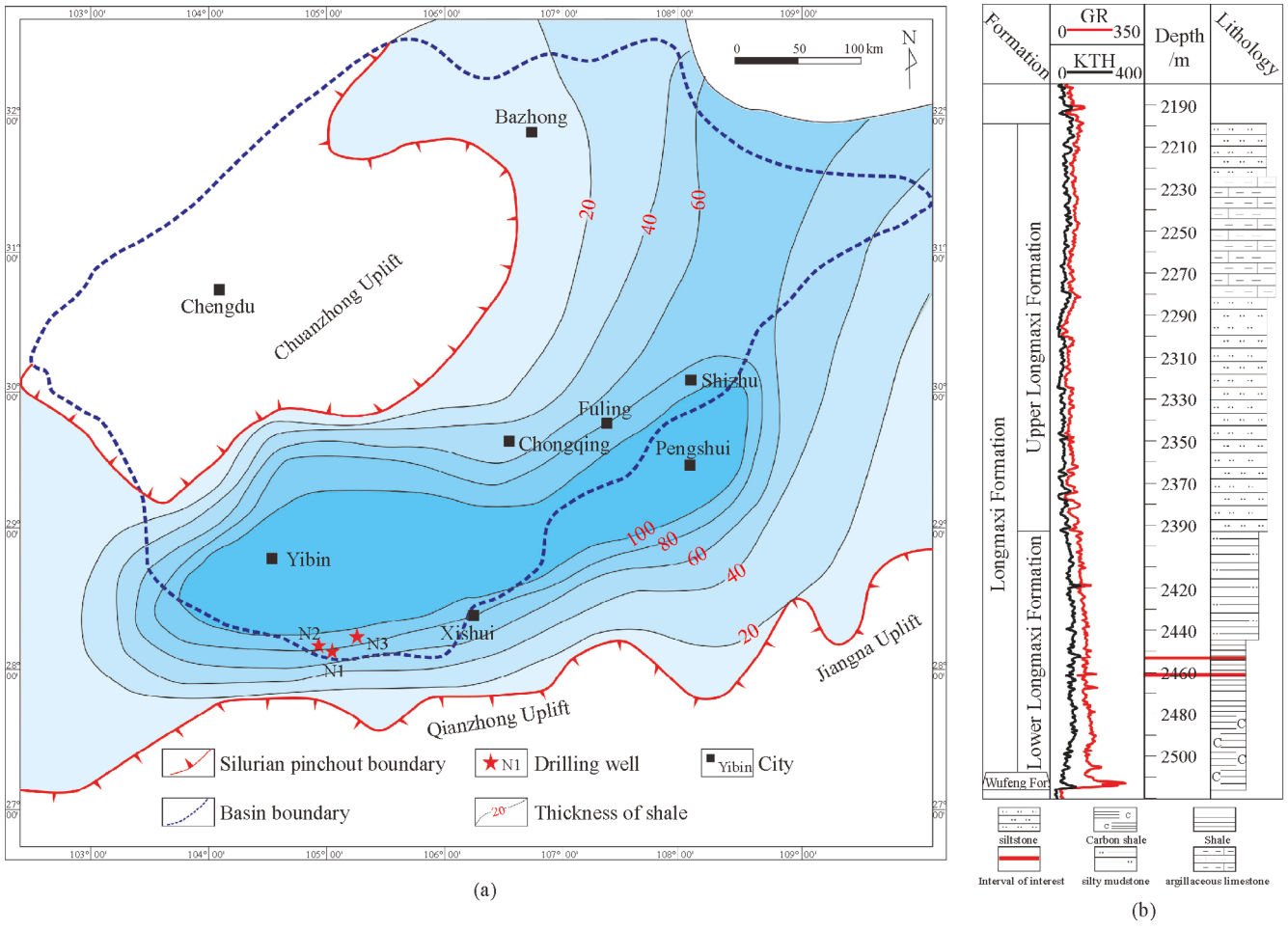

Fig. 1 (a) The thickness contour of the Longmaxi shale in the Sichuan Basin and the location of the drilling wells N1, N2 and N3 (Guo and Zhang, 2014). (b) Lithology column of the Wufeng Formation to the Longmaxi Formation in the N1 well.

3 Data and methods

This study is focused on the cores from two sections (Section-A: 2453.93−2454.25 m; Section-B: 2460.96−2461.54 m) of the Lower Member of the Longmaxi Formation in the Changning area of the South Sichuan Basin obtained from the N1 well. This study performed the description, thin section analysis, X-ray diffraction (XRD), major elements and trace elements test of these cores.

3.1 X-ray diffraction (XRD)

Seven samples from Section-A and ten samples from Section-B were selected for XRD test. The samples were crushed to a size of less than 1mm using a crushing machine, and grounded until the particle size was less than 40 μm using a grinder miller or agate mortar. Thereafter, the total mass of protolith powder of sedimentary rock was measured, and clay minerals with particle size less than 10 μm were extracted by suspension. The total amount of clay minerals was obtained by "Weighing Method", the content of each non-clay mineral was measured using the "K-value Method". For the test, the X-ray diffractometer was configured with a scanning angle of 5°−45°, step length of 0.02°, step speed of 2°/min, working voltage of 40 kV, and working current of 150 mA.

3.2 Major and trace elements test

For the major and trace elements test, dilithium tetraborate was used to melt the sample, ammonium nitrate was used as the oxidant, and lithium oxide and a small amount of lithium bromide were used as flux and mold release agent. An automatic fusion machine was utilized for fusion at a temperature range of 1150°C−1250°C, a glass sample wafer was made and measured with X-ray fluorescence spectrophotometer, and the contents of major and trace elements were calculated respectively according to fluorescence intensity.

3.3 Data calculations

To study the sedimentary environment of the siltstone-mudstone rhythmic sedimentary sections, the relevant parameters were calculated by using trace elements, and the specific calculation is as follows: influence of terrigenous detritus was eliminated through aluminum-standardization (Tribovillard et al., 2006).

Degree of enrichment of Mo and U are expressed using Mo-EF and U-EF, and the relevant formulas are: Mo-EF = (Mo-sample/Al-sample) / (Mo-average shale/Al-average shale); U-EF = (U-sample/Al-sample) / (U-average shale/Al-average shale) (Tribovillard et al., 2006).

Paleoclimate and weathering conditions were assessed by calculating the chemical index of alteration (CIA) using the following formula: $CIA = Al_2O_3/(Al_2O_3 + CaO^* + Na_2O + K_2O) \times 100$ (Nesbitt and Young, 1982; Price and Velbel, 2003), but they were omitted in the present study because of difficulty in measuring the CaO* content of calcareous sedimentary rocks (Liu et al., 2019).

4 Characteristics of siltstone-mudstone rhythmic sedimentary sections

4.1 Sedimentary structures

The lithology of siltstone-mudstone rhythmic sedimentary sections are characterized by interbedded layers of shale, silty shale, argillaceous siltstone and siltstone (Figs. 2 and 3). The laminas are well-developed in the siltstone-mudstone rhythmic sedimentary sections. A large number of rhythmic laminations composing of silt laminas and argillaceous laminas were developed with lamina thickness between 0.2 mm and 1.5 mm (Figs. 2 and 3). The shale layer mostly developed continuous horizontal rhythmic laminas (Figs. 3(a), 3(c) and 4(a)). Wavy laminas (Figs. 3(b) and 4(f)), boulder-clays (Fig. 4(b)) and deformation lamination (Fig. 4(c)) can be found in siltstone layer. The boulder-clays are oval in shape, with a size between 0.5 and 2.5 cm, and demonstrate a certain directional arrangement (Fig. 4(b)). The lithological interfaces of the

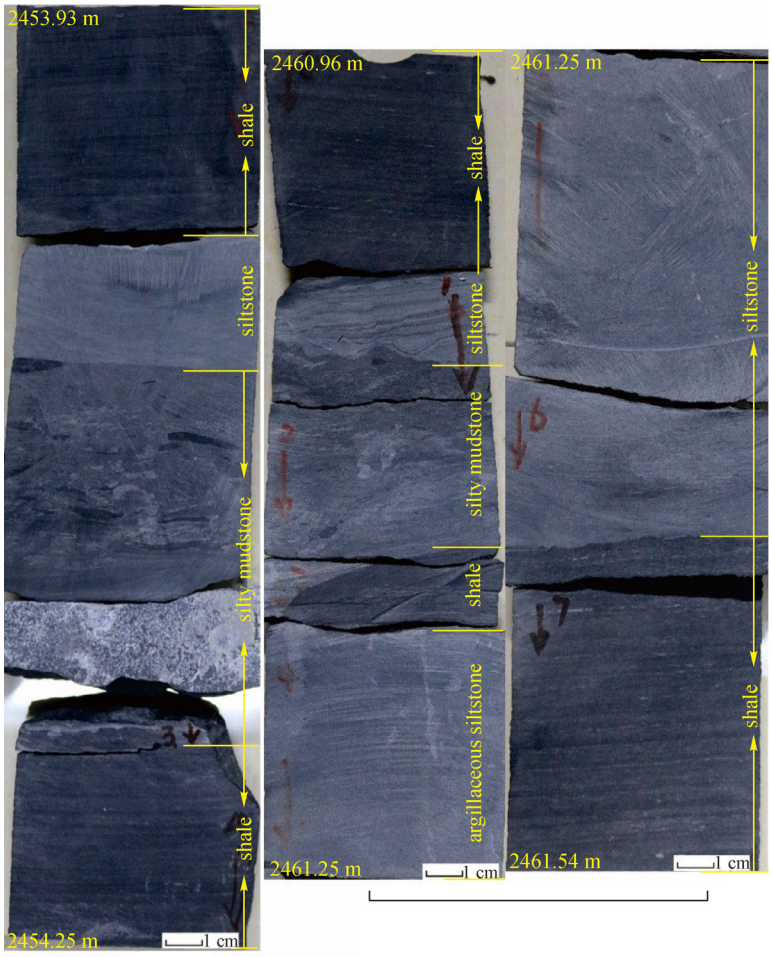

Fig. 2 Macroscopic characteristics of the siltstone-mudstone rhythmic sedimentary sections in the Lower Member of the Longmaxi Formation from the N1 well. (a): Section-A, 2453.93−2454.25 m; (b): Section-B, 2460.96−2461.54 m.

Fig. 3 Macroscopic characteristics of the siltstone-mudstone rhythmic sedimentary sections in the Lower Member of the Longmaxi Formation from the N2 well and N3 well. (a): Horizontal laminas developed in shale layer, 3124.63−3124.93 m, N2 well; (b).:Wave laminas developed in siltstone layer, 3105.04-3105.30 m, N2 well; (c): Shale and siltstone are in direct sharp contact, 3131.17−3131.52 m, N2 well; (d): Silty strips had developed in high frequency, 2063.15−2063.42 m, N3 well.

siltstone-mudstone rhythmic sedimentary sections are obvious and exhibit various forms, including direct sharp contact (Figs. 3(c) and 4(b)), oblique crossing contact (Fig. 4(g)), wavy contact (Figs. 3(d) and 4(c)) and gradual contact (Fig. 4(d)). In addition, small scouring surface (Fig. 4(c)), flamelike structure (Fig. 4(e)), lenticle (Fig. 4(d)) and bioturbated structures (Fig. 5(f)) can be found in the siltstone-mudstone rhythmic sedimentary sections.

Thin section analysis show that the siltstone-mudstone rhythmic sections are characterized by the development of various types of laminas, including horizontal laminas, rhythmic laminas, and wavy laminas. Horizontal laminas are mainly developed in the black shale, which are argillaceous laminas with a thickness of about 0.3 mm (Fig. 5(e)). Rhythmic laminas feature silty laminas interbedded with argillaceous laminas. The thickness of silty laminas differs greatly, ranging from 0.1 to 2 mm, while that of argillaceous laminas varies little, ranging from 0.2 to 0.5 mm. In addition to silty laminas interbedded with argillaceous laminas of equal thickness, the rhythmic laminas also show a pattern of thick silty laminas interbedded with thin argillaceous laminas, and silty laminas with varying thicknesses in the vertical direction (Figs. 5(a) and 5(h)). In addition, boulder-clays (Fig. 5(c)), flamelike structures (Fig. 5(d)) and bioturbated structures (Fig. 5(f)) could also be found.

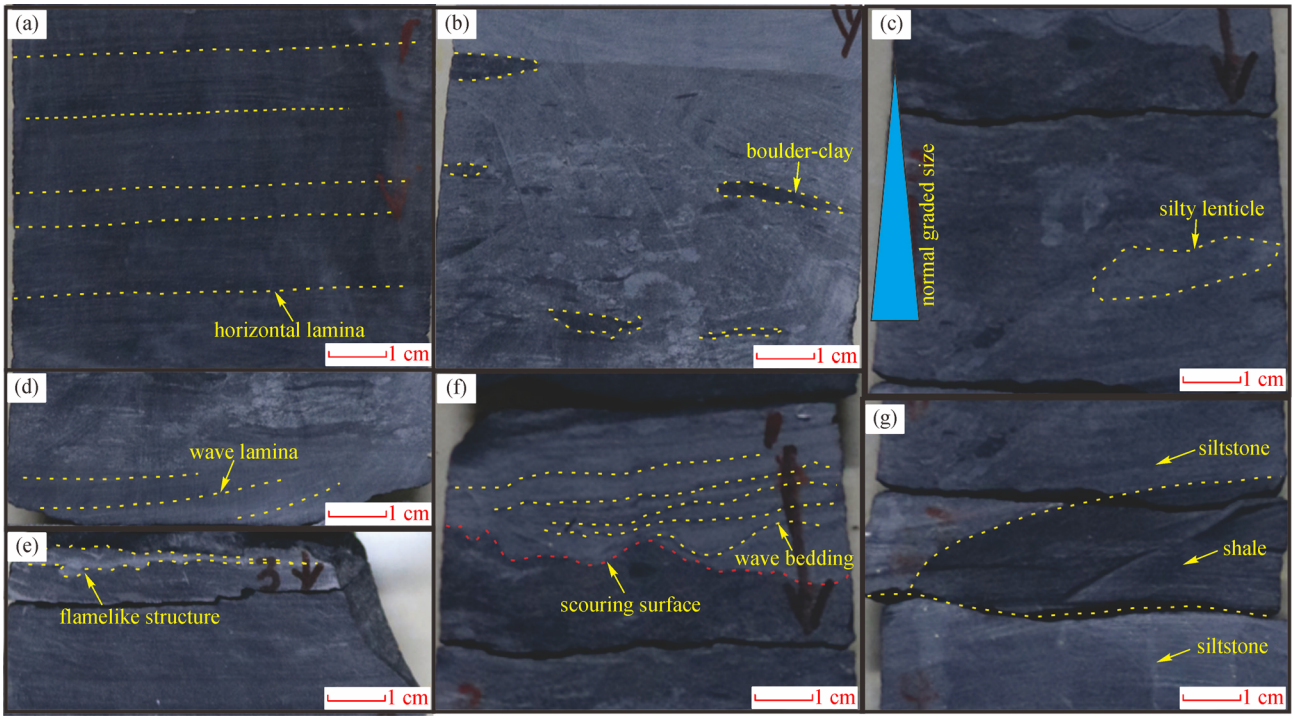

Fig. 4 Sedimentary structures of the siltstone-mudstone rhythmic sedimentary sections in the Lower Member of the Longmaxi Formation from the N1 well. (a) Rhythmic laminas developed in shale layer, 2453.93−2453.99 m. (b) Boulder-clays developed in siltstone layer, 2454.05−2454.12 m. (c) Shale and siltstone in gradual contact. Silty lenticle developed in silty mudstone, and obvious gradation from coarser to finer, 2461.08−2461.14 m. (d) Wave laminas developed in the siltstone layer, 2450.11−2540.13 m. (e) The flamelike structure developed in the top of shale layer, 2454.17−2454.19 m. (f) Wave laminas developed in siltstone layer, with thickness ranging from 0.05 mm to 0.25 mm. A small scouring surface can be observed at the bottom of siltstone. Siltstone in abrupt contact with shale, showing wavy interface, 2461.04−2461.09 m. (g) Oblique interface between siltstone and shale can be found, 2461.13−2461.17 m.

4.2 Sedimentary sequence of the silty-mudstone rhythmic sedimentary sections

The total length of Section-A is 0.32 m, and distributed within are, in sequence from bottom to top, 0.2 m dark-gray shale (A-1), 0.04 m light-gray siltstone (A-2) and 0.08 m dark-gray shale (A-3) (Fig. 6(a)). Looking from the bottom, up, Section A-1 shows lithology changing from shale to silty shale, color gradually becoming lighter, an increase in silty content and a rise in coarseness, while the laminas gradually changed from argillaceous laminas to silty laminas and from horizontal laminas to wavy cross laminas. The flamelike structure caused by differential compaction can be found in the middle part of Section A-1 and the boulder-clays in the silty mudstone is observed in the upper part of Section A-1. Meanwhile, Section A-2 is dominated by light-gray massive siltstone with a sharp contact that forms the Section A-1. The lithology of Section A-3 is mostly dark-gray shale with an abundance of horizontal laminas.

The total length of Section-B is 0.58 m, and distributed within are, in sequence from bottom to top, 0.15 m dark-gray shale (B-1), 0.35 m gray silty mudstone-siltstone (B-2) and 0.08 m gray black shale (B-3) (Fig. 6(b)). Dark-gray shale dominates Section B-1 with plentiful laminas having developed. Argillaceous laminas constitute the main staple in this section while silty laminas are occasionally observed. Looking at Section B-1 from the bottom up, the color becomes darker and clay content increases in. The lithological interfaces between Section B-1 and Section B-2 are obvious. Section B-2 is mostly comprised of silty mudstone and siltstone. While its clay content exhibits an increasing trend and then a decreasing when viewed from the bottom up, and argillaceous wavy laminas are developed in middle part of Section B-2. Lithology changes frequently from 2461.17 to 2461.04 m, with black-gray shale, gray silty shale and gray siltstone developing successively from the bottom up and the oblique or wavy lithological interfaces between these three kinds of lithology are obvious. Boulder-clays and silty lenticle could be found in the silty shale, and wavy bedding can be seen in siltstone. Gray-black shale are developed in Section B-3 with horizontal laminas having formed.

4.3 Geochemical characteristics of siltstone-mudstone characteristics of siltstone-mudstone rhythm sections

The siltstone-mudstone rhythmic sedimentary sections are

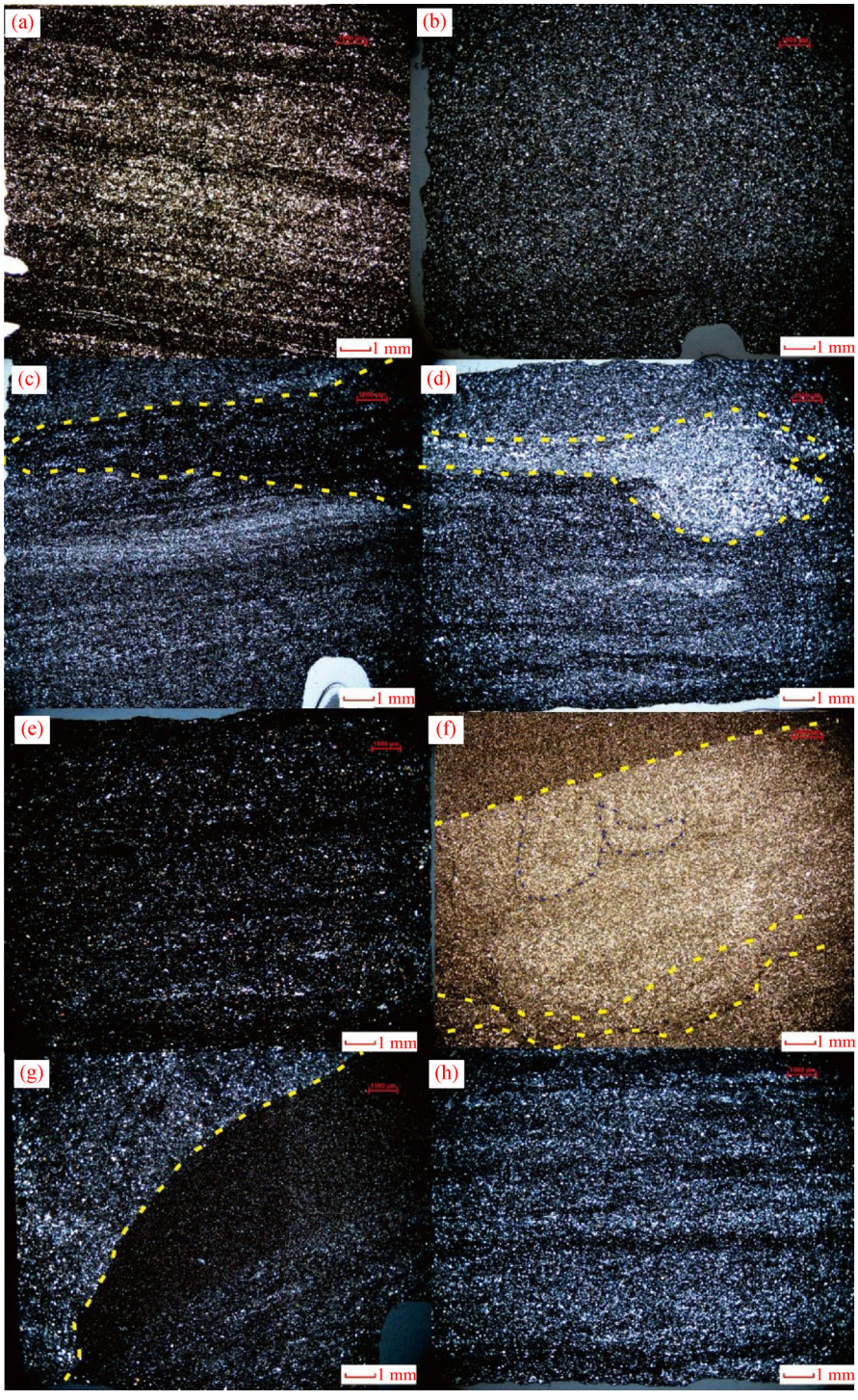

Fig. 5 Thin section showing characteristics of siltstone-mudstone rhythmic sedimentary sections in the Lower Member of the Longmaxi Formation from the N1 well. (a) Horizontal rhythmic laminas developed and silty laminas are thick, with thickness reaching up to about 1.5 mm. Silty laminas gradually thickened from the bottom up. Argillaceous laminas are thin, with thickness about 0.5 mm, 2453.96 m. (b) Obvious boundary between shale and siltstone, 2454.05 m. (c) Silty boulder-clays and silty laminas in argillaceous siltstone and the thickness of silty laminas are about 1.5 mm, 2454.08 m. (d) Flamelike structure and argillaceous lenticle were found in the shale, and the size of the lenticle was about 2 × 0.5 mm, 2454.17 m. (e) Argillaceous horizontal laminas developed with a thickness about 0.25 mm, 2460.98 m. (f) Wavy boundary between siltstone and shale, and bioturbated structures can be seen in siltstone, 2461.07 m. (g) Lithologic interface of shale and siltstone is oblique crossing, 2461.16 m. (h) Horizontal rhythmic laminas. Thickness of the argillaceous laminas are uniform with thickness about 0.3 mm, while the silty laminas show a gradually thinning trend from the bottom up with thickness between 1 mm and 2 mm, 2161.48 m.

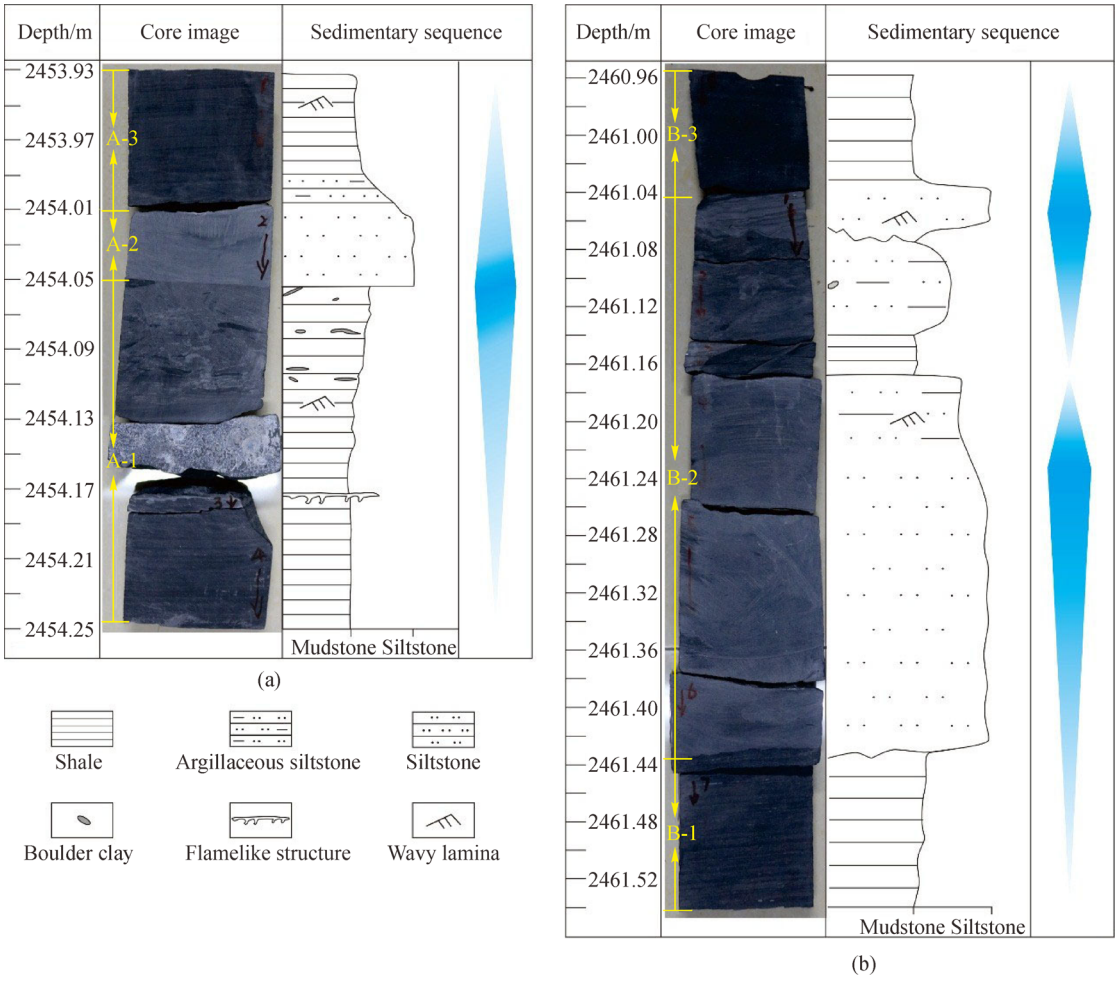

Fig. 6 Sedimentary sequences of siltstone-mudstone rhythmic sedimentary sections in the Lower Member of the Longmaxi Formation from the N1 well.

mainly composed of SiO_2, Al_2O_3 and CaO and the sum of these three components add up to 80.32% (Table 1). The content of SiO_2 in Section-A was higher than that in Section-B, respectively in the ranges of 53.08%−58.41% and 35.94%−63.58%, with the respective average values of 56.04% and 43.42%. Al_2O_3 content in these two sections are similar, respectively in the ranges of 6.25%−14.22% and 4.80%−12.64% with respective average values of 10.76% and 7.26%. CaO content in Section-A was lower than that in Section-B, respectively in the ranges of 6.20%−13.73% and 4.10%−17.88%, with the respective average values of 9.55% and 14.41%. Other than the three main components, Fe_2O_3, MgO, K_2O and Na_2O were also identified. The Fe_2O_3 contents of Section-A and Section-B are respectively in the ranges of 4.19%−5.13% and 4.10%−6.41%, with the respective mean values of 4.71% and 5.78%. The MgO contents of Section-A and Section-B are respectively in the ranges of 2.82%−4.13% and 3.05%−8.33%, with the respective mean values of 3.28% and 6.96%. The K_2O contents of Section-A and Section-B are respectively in the ranges of 1.06%−3.78% and 1.08%−3.24%, with the respective mean values of 2.54% and 1.77%. The Na_2O contents of Section-A and Section-B are respectively in the ranges of 1.33%−1.70% and 0.74%−1.56%, with the respective mean values of 1.47% and 1.03%. MnO_2 contents and TiO_2 contents are less than 1.0%, while the content of P_2O_5 is about 0.1%. Compared with the Average Shale (Tribovillard et al., 2006), the Al_2O_3 content in siltstone-mudstone rhythm sections is higher, indicating that there may be an influence of terrigenous clastic material input.

Only the authigenic trace elements in the sediments can accurately determine the palaeoenvironment. Therefore, the effect of terrestrial components in the trace elements in sediments should be removed, and a common method adopted in this regard is Al-standardization (Tribovillard et al., 2006). After the standardization of trace elements, the comparison with the world average shale (AS) is shown in Figs. 7 and 8. Mo, U and Ba in the siltstone-mudstone rhythmic sedimentary sections of the Lower

Table 1 Statistics of major elements in the siltstone-mudstone rhythmic sedimentary sections in the Lower Member of the Longmaxi Formation of N1 well

Sample	Depth/m	Lithology	Na_2O	MgO	Al_2O_3	SiO_2	MnO_2	K_2O	CaO	TiO_2	P_2O_5	Fe_2O_3
A-1	2454.00	shale	1.31	2.82	14.09	57.49	0.05	3.78	6.69	0.67	0.11	4.19
A-2	2454.03	siltstone	1.62	4.13	6.25	53.08	0.19	1.06	13.73	0.27	0.09	4.51
A-3	2454.08	shale	1.46	3.50	9.65	53.91	0.13	2.06	11.34	0.42	0.11	4.67
A-4	2454.12	shale	1.33	3.30	12.84	53.68	0.08	3.05	9.00	0.62	0.11	5.13
A-5	2454.18	shale	1.70	3.42	6.16	57.77	0.17	1.06	11.91	0.30	0.09	4.93
A-6	2454.19	shale	1.46	2.95	12.11	58.41	0.08	3.05	7.99	0.60	0.11	4.84
A-7	2454.21	shale	1.40	2.85	14.22	57.92	0.05	3.72	6.20	0.67	0.11	4.67
Average			1.47	3.28	10.76	56.04	0.11	2.54	9.55	0.50	0.11	4.71
Sample	Depth/m	Lithology	Na_2O	MgO	Al_2O_3	SiO_2	MnO_2	K_2O	CaO	TiO_2	P_2O_5	Fe_2O_3
B-1	2461.02	shale	1.20	4.27	12.54	54.92	0.11	3.29	6.99	0.60	0.11	5.43
B-2	2461.06	siltstone	0.93	7.98	6.52	37.80	0.28	1.54	16.72	0.32	0.09	6.27
B-3	2461.11	shale	0.93	8.33	5.52	36.69	0.30	1.29	17.84	0.27	0.09	6.43
B-4	2461.14	shale	0.74	8.30	7.37	35.94	0.27	1.89	16.88	0.32	0.09	6.30
B-5	2461.17	siltstone	0.89	8.17	4.80	37.61	0.32	1.08	17.88	0.23	0.07	6.41
B-6	2461.21	siltstone	0.86	8.23	5.04	37.74	0.30	1.14	17.88	0.23	0.07	6.06
B-7	2461.24	siltstone	0.90	8.05	5.16	38.64	0.30	1.16	17.50	0.23	0.07	6.04
B-8	2461.35	siltstone	1.02	7.67	5.48	40.44	0.28	1.24	16.74	0.25	0.09	5.86
B-9	2461.40	siltstone	1.21	5.52	7.59	51.81	0.19	1.81	11.62	0.37	0.09	4.94
B-10	2461.44	shale	1.56	3.05	12.64	63.58	0.06	3.23	4.10	0.58	0.11	4.10
Average			1.03	6.96	7.26	43.52	0.24	1.77	14.41	0.34	0.09	5.78

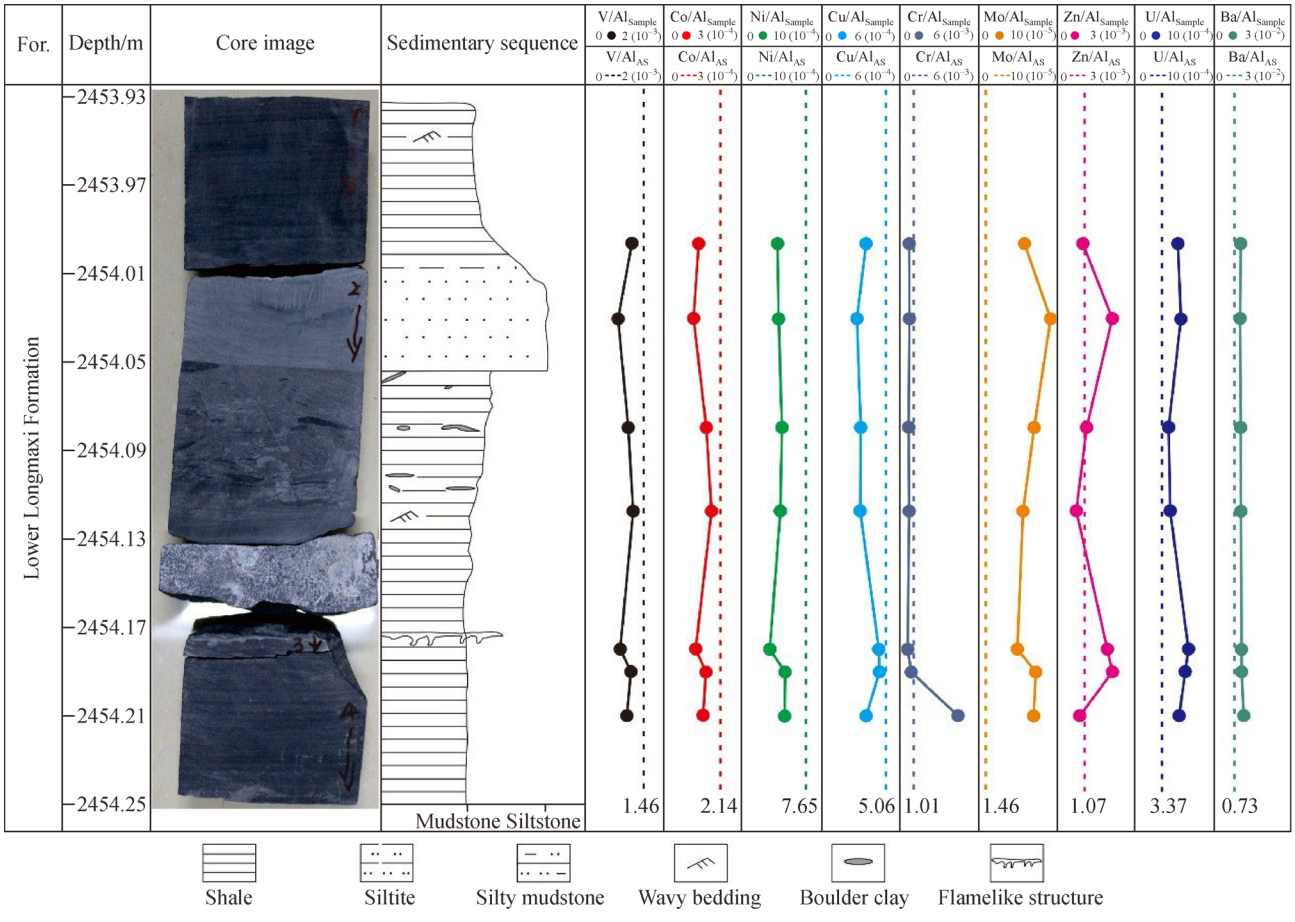

Fig. 7 Vertical variations of Al-standardized trace elements of Section-A in Lower Member of the Longmaxi Formation of N1 well.

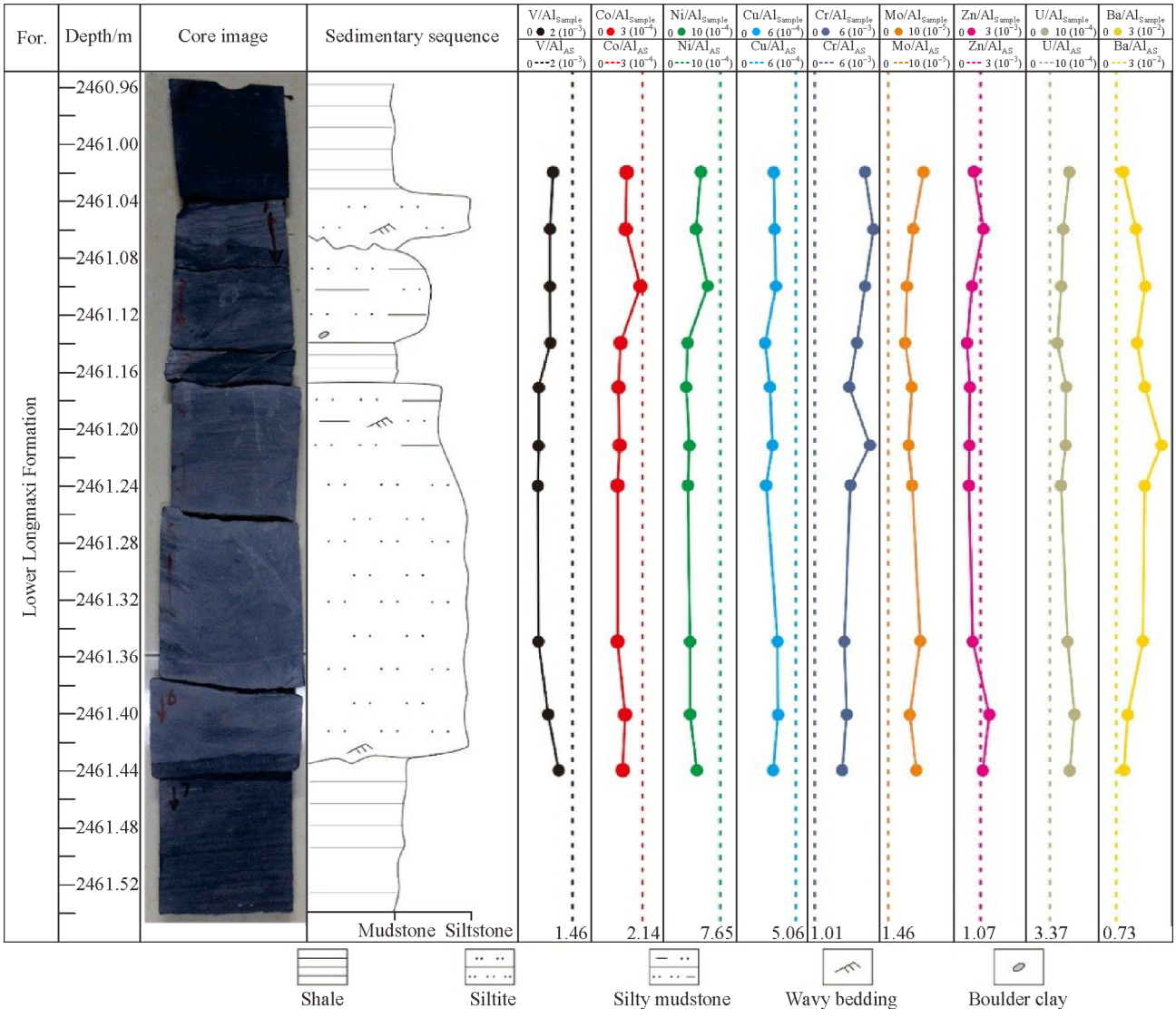

Fig. 8 Vertical variations of Al-standardized trace elements of Section-B in Lower Member of the Longmaxi Formation.

Member of the Longmaxi Formation are all higher than the world average shale, showing an obvious abundance. The content variation of Mo ranges from 1.04−5.04 μg/g with an average of 2.88 μg/g. The content of U spans from 1.33 to 4.22 μg/g and the average value figure is 2.61 μg/g. Ba content varies from 325.0 μg/g to 861 μg/g with an average value of 599.27 μg/g. The content of V, Co, Ni and Cu in the siltstone-mudstone rhythmic sedimentary sections of the Lower Member of the Longmaxi Formation are lower than the world average shale. The content variation of V is 13.5−88.1 μg/g with an average of 47.82 μg/g, while the content variation of Co is 3.02−12.9 μg/g with an average of 22.33 μg/g. The content variation of Cu is 6.79−25.9 μg/g with an average of 47.82 μg/g, while the content variation of Co is 3.02−12.9 μg/g with an average of 16.10 μg/g. Compared with the shale layer, the siltstone layer has lower V, Co and Ni contents (Table 2).

5 Discussion

5.1 Hydrodynamic condition

For marine shale, effects of hydrodynamics will gradually weaken with the increase of seawater depth because of lower seawater temperature, decreasing oxygen content and fewer biological disturbance (Wang et al., 2014b). In general, strong hydrodynamic conditions correspond to a relatively shallower, oxygen-rich, warmer and suitable environment, while weak hydrodynamic conditions are typically found at relatively deeper, anoxic and colder environment (Wang et al., 2014b). Relatively weak hydrodynamic condition is seen in the shale layer, which is mainly comprised of suspended deposition (Wang et al., 2014b). Suspended clay and silt particles sank to the bottom of the sea and formed horizontal laminas, which

Table 2 Statistics of trace elements in the siltstone-mudstone rhythmic sedimentary sections in the Lower Member of the Longmaxi Formation from the N1 well

Sample	Depth/m	Lithology	V	Co	Ni	Cu	Rb	Sr	Mo	Ba	Th	U	Cr
A-1	2454.00	shale	88.10	10.40	34.50	25.90	148.00	155.00	5.04	773.00	15.80	3.92	64.50
A-2	2454.03	siltstone	27.90	3.82	15.60	9.38	43.30	304.00	3.14	325.00	8.48	1.87	30.90
A-3	2454.08	shale	55.50	8.57	25.60	16.10	91.30	236.00	3.57	524.00	10.70	2.29	44.10
A-4	2454.12	shale	85.40	12.90	33.10	20.50	126.00	187.00	3.99	716.00	14.00	3.25	60.40
A-5	2454.18	shale	28.40	4.35	11.80	14.60	46.00	262.00	1.64	358.00	8.76	2.18	21.90
A-6	2454.19	shale	77.10	10.70	33.80	29.00	129.00	187.00	4.87	693.00	18.40	4.06	63.00
A-7	2454.21	shale	80.70	11.40	39.00	25.40	157.00	150.00	5.40	861.00	18.00	4.05	345.00
Average			63.30	8.88	27.63	20.13	105.80	211.57	3.95	607.14	13.45	3.09	89.97
Sample	Depth/m	Lithology	V	Co	Ni	Cu	Rb	Sr	Mo	Ba	Th	U	Cr
B-1	2461.02	shale	63.90	10.50	34.40	21.70	131.00	179.00	3.87	730.00	15.60	4.22	530.00
B-2	2461.06	siltstone	27.50	5.14	15.50	11.60	69.80	274.00	1.62	551.00	7.89	1.78	311.00
B-3	2461.11	shale	22.10	6.16	18.10	10.20	60.10	294.00	1.18	577.00	6.53	1.45	209.00
B-4	2461.14	shale	30.70	5.22	14.70	10.10	88.50	253.00	1.30	631.00	7.56	1.58	249.00
B-5	2461.17	siltstone	13.50	3.09	9.83	8.00	49.50	283.00	1.04	666.00	6.66	1.33	217.00
B-6	2461.21	siltstone	18.00	3.06	8.52	7.11	52.50	302.00	1.21	517.00	7.81	1.40	161.00
B-7	2461.24	siltstone	17.40	3.02	9.20	6.79	53.20	306.00	1.31	519.00	6.85	1.36	168.00
B-8	2461.35	siltstone	19.00	3.23	11.20	10.00	53.30	302.00	1.50	495.00	7.59	1.56	145.00
B-9	2461.40	siltstone	34.10	5.92	15.50	14.10	74.70	230.00	1.72	502.00	10.90	2.74	220.00
B-10	2461.44	shale	77.20	9.10	32.70	21.10	144.00	140.00	3.31	726.00	16.10	3.89	325.00
Average			32.34	5.44	16.97	12.07	77.66	256.30	1.81	591.40	9.35	2.13	253.50

have been preserved because of the absence of influence form bottom current and bioturbation.

Sand-body reshaped by bottom current could be identified by primary sedimentary structures, and the tractive structure is the only reliable source to identify sand-bodies reshaped by bottom current (Shanmugam, 2000, 2011; Zhao et al., 2017). Unlike turbidite deposit, siltstone deposited by the bottom current usually features a top interface that makes abrupt contact with the overlying strata, and also develops an internal erosion interface (Zhao et al., 2017). The rhythmic laminas (Fig. 4(a)), wavy laminas (Fig. 4(e)), small scouring surface (Fig. 4(c)) and directional arrangement of boulder-clays can be seen in the siltstone-mudstone rhythmic sedimentary sections (Fig. 4 (b)), which are all the products of tractive current (Shanmugam, 2011; Zhao et al., 2016). In addition, the abrupt interface between shale and siltstone (Figs. 4(b), 4 (f) and 4(g)) shows that there were sudden changes in hydrodynamics. Therefore, the siltstone layer in siltstone-mudstone rhythmic sedimentary sections were deposited under a relatively strong hydrodynamic conditions involving bottom current, and bottom current contributed to the formation of the siltstone.

5.2 Palaeoredox conditions

U, V, Ni, Mo, Th and Cr are reliable indices to interpret palaeoredox conditions (Jones and Manning, 1994), with Ni and Co often employed as redox index. High Ni/Co ratio (>7.0) corresponds to a reducing atmosphere, and a Ni/Co ratio of 5.0−7.0 indicates an anoxic atmosphere, while low Ni/Co ratio (<5.0) correlates to anoxic atmosphere (Jones and Manning, 1994). Ni/Co values vary from 2.57 to 4.08 with an average of 3.18 in Section-A, and range from 2.78 to 3.59 with an average of 3.07 in Section-B, with all values pointing to an oxic atmosphere. The U/Th ratio is also a reliable redox index. High values of U/Th (>1.25) indicate an anoxic atmosphere, and low values of U/Th (<0.75) represent an oxic atmosphere, while a U/Th ratio between 0.75 and 1.25 is linked to a dysoxic atmosphere (Wilkin et al., 1997). There is little change between the U/Th ratios of Section-A and Section-B, which respectively range from 0.21 to 0.25 and 0.18 to 0.27, with respective averages of 0.23 and 0.22, meaning that the environment had an oxic atmosphere. The values of $V/(V+Ni)<0.46$ are thought to represent oxic depositional conditions. Values ranging from 0.46 to 0.57 are indicative of the weak-oxidizing depositional conditions, while values between 0.57 and 0.83 suggest dysoxic-anoxic depositional conditions, and values between 0.83 and 1 are understood as indicator of euxinic environment (Wingenall, 1994). The values of $V/(V+Ni)$ range from 0.64 to 0.72 with an average of 0.69 in Section-A, while Section-B data range from 0.55 to 0.70 with an

average of 0.64. All data reflect that the depositional environment had a dysoxic-oxic condition. Furthermore, V/Cr has also been used as a redox index. Low values (V/Cr < 2) imply oxic conditions, values ranging from 2 to 4.25 designate dysoxic conditions, and a high value (V/Cr > 4.25) represents anoxic conditions (Jones and Manning, 1994). Values of V/Cr were between 0.23 and 1.41 with an average of 1.10 in Section-A, while values range from 0.06 to 0.24 with an average of 0.12 in Section-B. All values of V/Cr indicate an oxic environment. According to the four redox indexes, oxic conditions prevailed in the palaeoenvironment of the siltstone-mudstone rhythm sections in the Lower Member of the Longmaxi Formation (Figs. 9 and 10).

The cross plot of Mo-U shows that the values of Mo/U in siltstone-mudstone rhythmic sedimentary sections are mainly between 0.3 × SM and SM, except two data from section-A slightly higher than SM. Which indicates that the siltstone-mudstone rhythmic sedimentary sections are formed in the oxic environment with the anoxic environment occasionally happened during the depositional process (Fig. 11).

The CIA value can be used as a proxy for interpreting the intensity of chemical weathering in the provenance (Young and Nesbitt, 1998). Sediments deposited in cold and arid climates have CIA values from 50 to 70, those in a warm and humid climate have CIA values of 70−80, and CIA values of 80−100 correspond to hot and humid climate (Nesbitt and Young, 1982; Liu et al., 2019; Yan et al., 2010). The CIA values are between 69.96 and 74.46 with an average of 72.44 in section-A, while between 70.74 and 73.67 with an average of 71.97 in section-B. All data from CIA values indicate the warm and humid paleoclimate during the depositional period of the siltstone-mudstone rhythm (Figs. 9 and 10).

5.3 Sedimentary model

Sea level fell due to the Gondwana glacier event during the late depositional stage of the Wufeng Formation (Couto et al., 2013). The sedimentary environment transformed from deep water and anoxic environment during the early depositional stage of the Wufeng Formation to the shallow and oxic environment during the late depositional stage of the Wufeng Formation, resulting in sediments that changed from organic-rich shale to bioclastic limestone or bioclastic

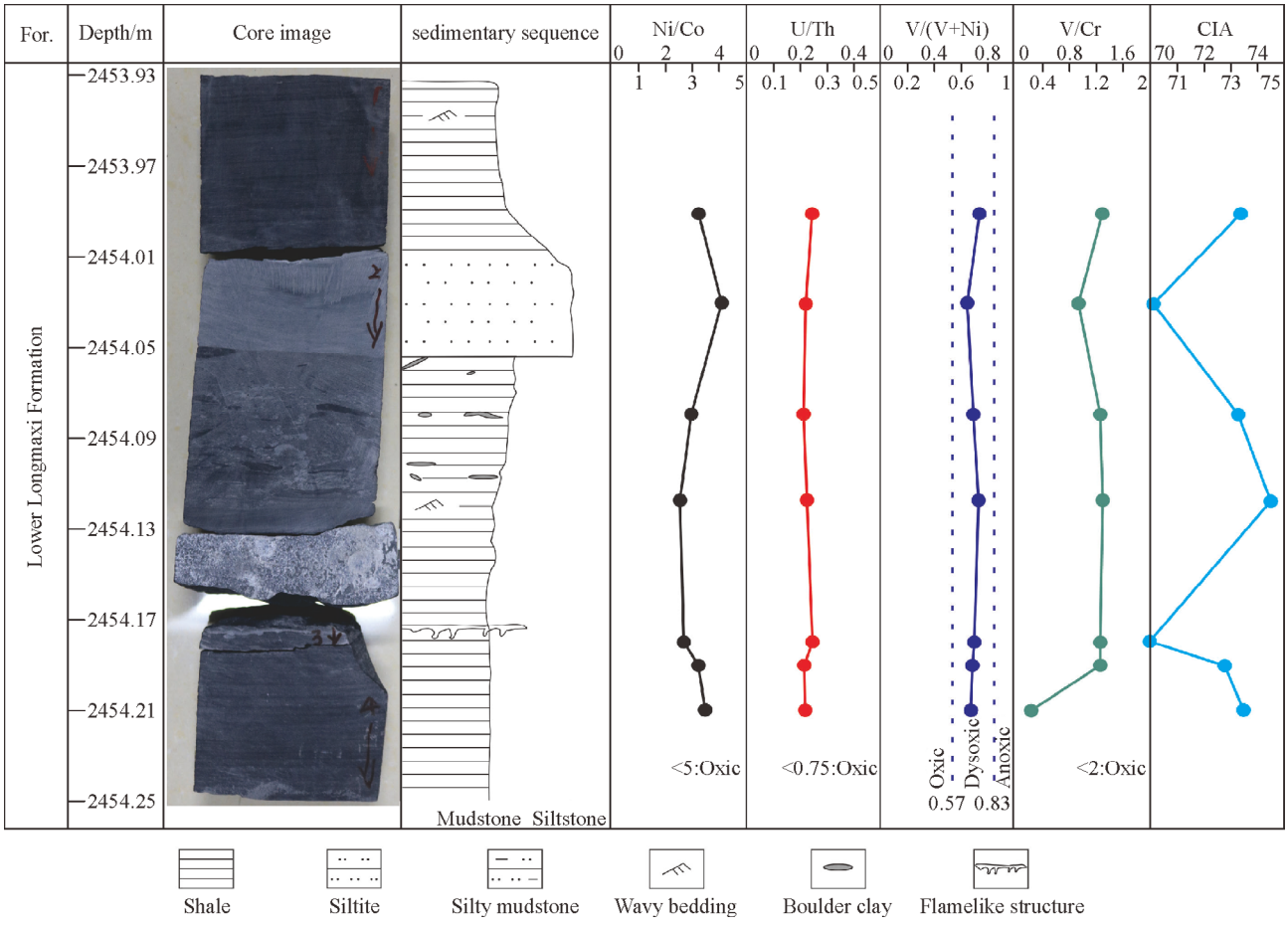

Fig. 9 Redox index and CIA values of the Section-A in the Lower Member of the Longmaxi Formation from the N1 well.

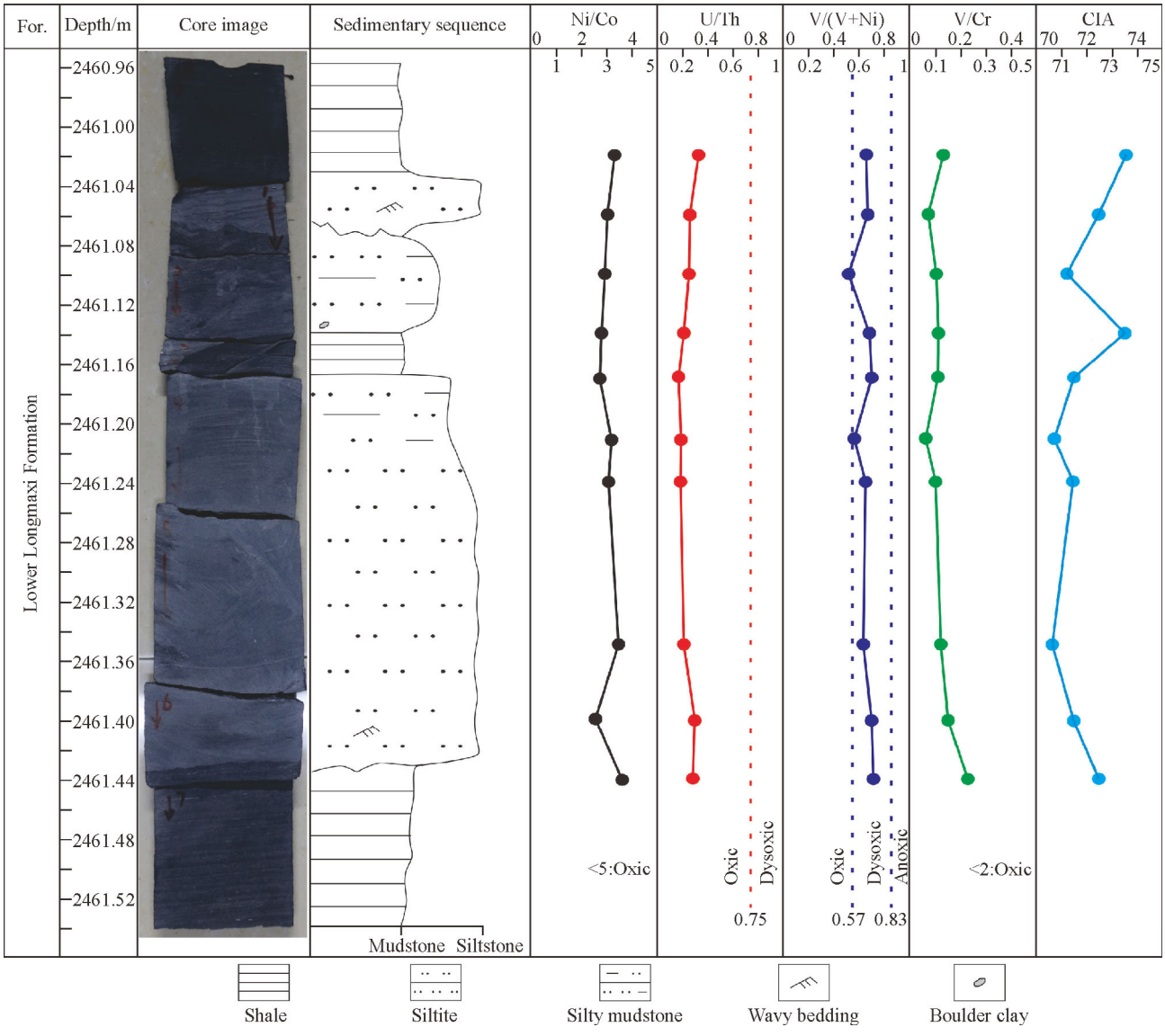

Fig. 10 Redox index and CIA values of Section-B in the Lower Member of the Longmaxi Formation from the N1 well.

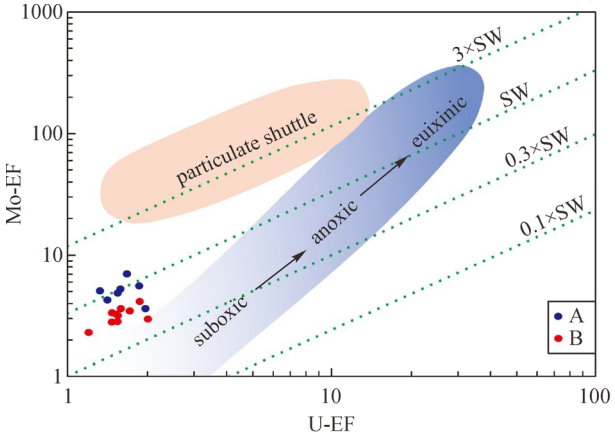

Fig. 11 Cross plot of Mo-EF versus U-EF for the siltstone-mudstone rhythmic sedimentary sections in the Lower Member of the Longmaxi Formation from the N1 well. Particulate shuttle and redox fields from Algeo and Tribovillard (2009).

mudstone (Zhang et al., 2019). In the early depositional stage of the Longmaxi Formation, sea level rose as a result of the melting of the Gondwana glacier, dysoxic-anoxic deep water shelf dominated the majority of the Sichuan Basin area, leading to a broad distribution of organic-rich shales (Fig. 12(a)) (Wang et al., 2014b; Chen et al., 2004; Chen et al., 2015b). As the sea level dropped, the oxygen content of water column increased as a result of the influence of deep water bottom current and terrigenous supply, which led to the development of siltstone-mudstone rhythmic sedimentary sections (Fig. 12(b)). Subsequently, the sedimentary environment gradually changed to an oxic environment due to the continuous decline of sea level, with gray argillaceous siltstone and siltstone depositing in the Upper Member of the Longmaxi Formation (Rong et al., 2019).

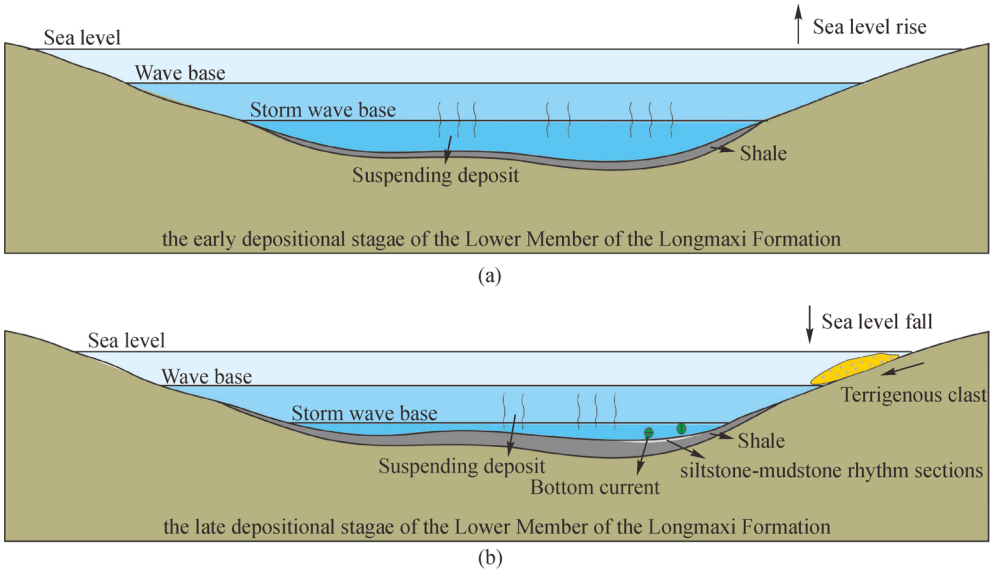

Fig. 12 Sedimentary model of siltstone-mudstone rhythmic sedimentary sections in the Lower Member of the Longmaxi Formation of Changning area.

6 Conclusions

The two siltstone-mudstone rhythmic sedimentary sections of the Longmaxi Formation in the Changning area analyzed from samples of the N1 well are characterized by frequent interbed between gray-black shale and light-gray siltstone. Argillaceous laminas and silty laminas are well developed in siltstone-mudstone rhythmic sedimentary sections. The shale layer mainly features well-developed horizontal rhythmic laminas, while the siltstone layer has well-developed wavy laminas. The major compositional elements are SiO_2, Al_2O_3 and CaO, followed by Fe_2O_3, MgO, K_2O and Na_2O. Compared with the world average shale, the siltstone-mudstone rhythmic sedimentary sections are rich in Mo, U and Ba but loss in V, Co, Ni and Cu. Compared with shale, siltstone has lower V, Co and Ni values. The geochemical redox indices, Mo-U and CIA values suggest the formation of the siltstone-mudstone rhythmic sedimentary sections are related to the influence of bottom current in oxic conditions with a warm and humid paleoclimate.

Acknowledgements This study was supported by the National Natural Science Foundation of China (Grant No. 41602147) and Science and Technology Cooperation Project of the CNPC-SWPU Innovation Alliance (No. 2020CX020000).

References

Algeo T J, Marenco P J, Saltzman M R (2016). Co-evolution of ocean, climate, and the biosphere during the "Ordovician Revolution": a review. Palaeogeogr Palaeoclimatol Palaeoecol, 458: 1–11

Algeo T J, Tribovillard N (2009). Environmental analysis of paleoceanographic systems based on molybdenum-uranium covariation. Chem Geol, 268(3-4): 211–225

Aplin A C, Macquaker J H S (2011). Mudstone diversity: origin and implications for source, seal, and reservoir properties in petroleum systems. AAPG Bull, 95(12): 2031–2059

Chen L, Lu Y C, Jiang S, Li J Q, Guo T L, Luo C (2015a). Heterogeneity of the Lower Silurian Longmaxi marine shale in the southeast Sichuan Basin of China. Mar Pet Geol, 65: 232–246

Chen L, Wang G X, Yang Y, Jing C, Chen M, Tan X C (2019). Geochemical characteristics of bentonite and its influence on shale reservoir quality in Wufeng-Longmaxi Formation, south Sichuan Basin, China. Energ Fuel, 33(12): 12366–12373

Chen L, Lu Y C, Jiang S, Li J Q, Guo T L, Luo C, Xing F C (2015b). Sequence stratigraphy and its application in marine shale gas exploration: a case study of the Lower Silurian Longmaxi Formation in the Jiaoshiba shale gas field and its adjacent area in southeast Sichuan Basin, SW China. J Nat Gas Sci Eng, 27: 410–423

Chen L, Lu Y C, Li J Q, Guo X S, Jiang S, Luo C (2020). Comparative study on the Lower Silurian Longmaxi marine shale in the Jiaoshiba shale gas field and the Pengshui area in the southeast Sichuan Basin, China. Geosci J, 24(1): 61–71

Chen X, Rong J Y, Li Y, Boucot A J (2004). Facies patterns and geography of the Yangtze region, South China, through the Ordovician and Silurian transition. Palaeogeogr Palaeoclimatol Palaeoecol, 204(3-4): 353–372

Couto H, Knight J, Lourenco A (2013). Late Ordovician ice-marginal processes and sea-level change from the north Gongwana platform: Evidence from the Valongo Anticline (northern Portugal). Palaeogeogr Palaeoclimatol Palaeoecol, 375: 1–15

Dai J X, Zou C N, Liao S M, Dong D Z, Ni Y Y, Huang J L, Wu W, Gong D Y, Huang S P, Hu G Y (2014). Geochemistry of the extremely high thermal maturity Longmaxi shale gas, southern Sichuan Basin. Org Geochem, 74: 3–12

Drummond C, Sheets H (2001). Taphonomic reworking and stratal

organization of tempestite deposition: Ordovician Kope Formation, northern Kentucky, U.S.A. J Sediment Res, 71(4): 621–627

Guo T L, Zhang H R (2014). Formation and enrichment mode of Jiaoshiba shale gas field, Sichuan basin. Pet Explor Dev, 41(1): 31–40

Guo Y H, Li Z F, Li D H, Zhang T M, Wang Z C, Yu J F, Xi J T (2004). Lithofacies palaeogeography of the Early Silurian in Sichuan area. J Palaeogeogr, 6(1): 20–29 (in Chinese)

Han J, Cai Q S, Li Y, Li X W (2019). Forming environment and development model of high-quality marine shale: a case of the Wufeng-Longmaxi Formations shale in Zigui-Xintan section in the Middle Yangtze region. J Palaeogeogr, 21(04): 661–674 (in Chinese)

He T H, Lu S F, Li W H, Sun D Q, Pan W Q, Zhang B A, Tan Z Z, Ying J F (2020). Paleoweathering, hydrothermal activity and organic matter enrichment during the formation of earliest Cambrian black strata in the northwest Tarim Basin, China. J Petrol Sci Eng, 189: 106987

Jones B, Manning D A C (1994). Comparison of geochemical indices used for the interpretation of palaeoredox conditions in ancient mudstones. Chem Geol, 111(1–4): 111–129

Jiang S, Tang X L, Long S X, McLennan J, Jiang Z L, Jiang Z Q, Xu Z Y, Chen L, Xue G, Shi X, He Z L (2017). Reservoir quality, gas accumulation and completion quality assessment of Silurian Longmaxi marine shale gas play in the Sichuan Basin, China. J Nat Gas Sci Eng, 39: 203–215

Li Y Z, Wang X Z, Wu B, Li G Q, Wang D L (2016). Sedimentary facies of marine shale gas formations in Southern China: The Lower Silurian Longmaxi Formation in the Southern Sichuan Basin. J Earth Sci, 27(5): 807–822

Liang C, Jiang Z X, Cao Y C, Wu M H, Guo L, Zhang C M (2016). Deep-water depositional mechanisms and significance for unconventional hydrocarbon exploration: A case study from the lower Silurian Longmaxi shale in the southeastern Sichuan Basin. AAPG Bull, 100 (5): 773–794

Liu S G, Li Z B, Sun W, Deng B, Luo Z L, Wang G Z, Yong Z Q, Huang Q M (2011). Basic geological features of superimposed basin and hydrocarbon accumulation in Sichuan, China. Chinese J Geology, 46 (1): 233–257 (in Chinese)

Liu Y, Wu B, Gong Q S, Cao H Y (2019). Geochemical characteristics of the lower Silurian Longmaxi Formation on the Yangtze Platform, South China: implications for depositional environment and accumulation of organic matters. J Asian Earth Sci, 184: 104003

Lu Y B, Ma Y Q, Wang Y X, Lu Y C (2017). The sedimentary response to the major geological events and lithofacies characteristics of Wufeng Formation-Longmaxi Formation in the Upper Yangtze area. Earth Sci, 42(07): 1169–1184 (in Chinese)

Ma X H, Xie J (2018). The progress and prospects of shale gas exploration and development in southern Sichuan Basin, NW China. Pet Explor Dev, 45(1): 182–182

Ma Y Q, Fan M J, Lu Y C, Guo X S, Hu H Y, Chen L, Wang C, Liu X C (2016). Geochemistry and sedimentology of the Lower Silurian Longmaxi mudstone in southwestern China: implications for depositional controls on organic matter accumulation. Mar Pet Geol, 75: 291–309

Macquaker J H S, Bentley S J, Bohacs K M (2010). Wave-enhanced sediment gravity flows and mud dispersal across continental shelves: reappraising sediment transport processes operating in ancient mudstone successions. Geology, 38(10): 947–950

Nesbitt H M, Young G M (1982). Early Proterozoic climates and plate motions inferred from major element chemistry of lutites. Nature, 299 (5885): 715–717

Price J R, Velbel M A (2003). Chemical weathering indices applied to weathering profiles developed on heterogeneous felsic metamorphic parent rocks. Chem Geol, 202(3-4): 397–416

Qiu Z, Zou C N (2020). Unconventional petroleum sedimentary: connotation and prospect. Acta Sedimentol Sin, 38(01): 1–29 (in Chinese)

Rong J Y, Wang Y, Zhan R B, Fan J K, Huang B, Tang P, Li Y, Zhang X L, Wu R C, Wang G X, Wei X (2019). Silurian integrative stratigraphy and timescale of China. Sci China Earth Sci, 62(1): 89–111 (in Chinese)

Shan C A, Zhang T S, Wei Y, Zhang Z (2017). Gas shale reservoir characteristics of Ordovician−Silurian in the north of middle Yangtze area, China. Front Earth Sci, 11(1): 184–201

Shanmugam G (2011). New Perspectives on Deep-water Sandstone: Origin, Recognition, Initiation and Reservoir Quality. Burlington: Elsevier

Shanmugam G (2000). 50 years of the turbidite paradigm: deep-water processes and facies models: a critical perspective. Mar Pet Geol, 17 (2): 285–342

Shu Y, Lu Y C, Chen L, Wang C, Zhang B Q (2020). Factors influencing shale gas accumulation in the lower Silurian Longmaxi formation between the north and South Jiaoshiba area, Southeast Sichuan Basin, China. Mar Pet Geol, 111: 905–917

Smith L B, Schieber J, Wilson R D (2019). Shallow-water onlap model for the deposition of Devonian black shales in New York, USA. Geology, 47: 279–283

Su W B, Huff W D, Ettensohn F R, Liu X M, Zhang J E, Li Z M (2009). K-bentonite, black shale and flysh successions at the Ordivician-Silurian transition, South China: possible sedimentary responses to the accretion of Cathaysia to the Yangtze Block and its implications for the evolution of Gondwana. Gondwana Res, 15(1): 111–130

Tribovillard N, Algeo T J, Lyons T, Riboulleau A (2006). Trace metals as paleoredox and paleoproductivity proxies: an update. Chem Geol, 232(1−2): 12–32

Wang S F, Zou C N, Dong D Z, Wang Y M, Huang J L, Guo Z J (2014a). Biogenic silica of organic-rich shale in Sichuan Basin and its significance for shale gas. Acta Scuentiarum Naturalium Universitatis Pekinensis, 50(03): 476–486 (in Chinese)

Wang Y M, Dong D Z, Li X J, Huang J L, Wang S F, Wu W (2015). Stratigraphic sequence and sedimentary characteristics of Lower Silurian Longmaxi Formation in Sichuan Basin and its peripheral areas. Natural Gas Industry B, 2(2−3): 222–232 (in Chinese)

Wang Y M, Li X J, Dong D Z, Zhang C C, Wang S F, Huang J L, Guan Q Z (2016). Development mechanism of fracture pores in marine shale and its geological significance. Natural Gas Geoscien, 27(9): 1602–1610 (in Chinese)

Wang Z F, Zhang Y F, Liang X L, Cheng F, Jin Q H, Liu W, Zhang H B, Li H P (2014b). Characteristics of shale lithofacies formed under different hydrodynamic conditions in the Wufeng-Longmaxi Formation, Sichuan Basin. Acta Petrol Sin, 35(4): 623–632 (in Chinese)

Wilkin R T, Arthur M A, Dean W E (1997). History of water column

anoxia in the Black Sea indicated by pyrite framboids size distributions. Earth Planet Sci Lett, 148(3−4): 517–525

Wingenall P B (1994). Black Shales. Oxford: Clarendon Press

Yan C N, Jin Z J, Zhao J H, Du W, Liu Q Y (2018). Influence of sedimentary environment on organic matter enrichment in shale: a case study of the Wufeng and Longmaxi Formations of Sichuan Basin, China. Mar Pet Geol, 92: 880–894

Yan D T, Chen D Z, Wang Q C, Wang J G (2010). Large-scale climate fluctuations in the latest Ordovician on the Yangtze block, south China. Geology, 38(7): 599–602

Yan D T, Chen D Z, Wang Q C, Wang J G (2009). Geochemical changes across the Ordovician-Silurian transition on the Yangtze platform, South China. Sci China, 52(1): 38–54

Young G M, Nesbitt H M (1998). Processes controlling the distribution of Ti and Al in weathering profiles, siliciclastic sediments and sedimentary rocks. J Sediment Res, 68(3): 448–455

Zhang Y D, Zhan R B, Zhen Y Y, Wang Z H, Yuan F W, Fang X, Ma X, Zhang J P (2019). Ordovician integrative stratigraphy and timescale of China. Sci China Earth Sci, 62(1): 61–88 (in Chinese)

Zhao J H, Jin Z J, Jin Z K, Wen X, Geng Y K, Yan C N, Nie H K (2017). Depositional environment of shale in Wufeng and Longmaxi Formations, Sichuan Basin. Acta Petrol Sin, 2(3): 209–221

Zhao J H, Jin Z J, Jin Z K, Wen X, Yan C N, Nie H K (2016). Lithofacies types and sedimentary environment of shale in Wufeng-Longmaxi Formation, Sichuan Basin. Acta Petrol Sin, 37(5): 572–586

Zou C N, Dong D Z, Wang S J, Li J Z, Li X J, Wang Y M, Li D H, Cheng K M (2010). Geological characteristics and resource potential of shale gas in China. Pet Explor Dev, 37(6): 641–653

Zou C N, Dong D Z, Wang Y M, Li X J, Huang J L, Wang S F, Guan Q Z, Zhang C C, Wang H Y, Liu H L, Bai W H, Liang F, Lin W, Zhao Q, Liu D X, Yang Z, Liang P P, Sun S S, Qiu Z (2015). Shale gas in China: characteristics, challenges and prospects (I). Pet Explor Dev, 42(6): 753–767

Zou C N, Dong D Z, Wang Y M, Li X J, Huang J L, Wang S F, Guan Q Z, Zhang C C, Wang H Y, Liu H L, Bai W H, Liang F, Lin W, Zhao Q, Liu D X, Yang Z, Liang P P, Sun S S, Qiu Z (2016). Shale gas in China: characteristics, challenges and prospects (II). Pet Explor Dev, 43(2): 182–196